Refractivity estimation from sea clutter: An invited review

Ali Karimian,[1] Caglar Yardim,[1] Peter Gerstoft,[1] William S. Hodgkiss,[1] and Amalia E. Barrios[2]

Received 1 July 2011; revised 11 October 2011; accepted 12 October 2011; published 24 December 2011.

[1] Non-standard radio wave propagation in the atmosphere is caused by anomalous changes of the atmospheric refractivity index. In recent years, refractivity from clutter (RFC) has been an active field of research to complement traditional ways of measuring the refractivity profile in maritime environments which rely on direct sensing of the environmental parameters. Higher temporal and spatial resolution of the refractivity profile, together with a lower cost and convenience of operations have been the promising factors that brought RFC under consideration. Presented is an overview of the basic concepts, research and achievements in the field of RFC. Topics that require more attention in future studies also are discussed.

Citation: Karimian, A., C. Yardim, P. Gerstoft, W. S. Hodgkiss, and A. E. Barrios (2011), Refractivity estimation from sea clutter: An invited review, *Radio Sci.*, *46*, RS6013, doi:10.1029/2011RS004818.

1. Introduction

[2] Refractivity from clutter (RFC) techniques estimate the lower atmospheric refractivity structure surrounding a radar using its sea surface reflected clutter signal. The knowledge of the refractivity structure enables radar operators to compensate for non-standard atmospheric effects, or at least be aware of the radar limitations in specific locations. In the last decade, there has been interest in estimation of the environmental refractivity profile using the radar backscattered signals. RFC can be described as a fusion of two disciplines [*Rogers et al.*, 2000; *Gerstoft et al.*, 2003b; *Vasudevan et al.*, 2007]: numerical methods for efficient electromagnetic wave propagation modeling and estimation theory.

[3] Variations in the vertical refractivity profile can result in entrapment of the electromagnetic waves, creating lower atmospheric ducts. Ocean ducts are common phenomena that result in significant variations in the maximum operational radar range, creation of radar fades where the radar performance is reduced, and increased sea clutter [*Skolnik*, 2008]. Therefore, they greatly alter the target detection performance at low altitudes [*Anderson*, 1995], and result in significant height error for 3-D radars.

[4] RFC techniques find the profile associated with the best modeled clutter match to the observed clutter power. RFC has the advantage of temporal and spatial tracking of the refractivity profile in a dynamically changing environment.

[5] Atmospheric pressure, temperature and humidity affect the refractivity structure, and thus affect the radar propagation conditions. The vertical gradient of the refractivity profile determines the curvature of radar rays [*Doviak and Zrnić*, 1993]. Therefore, radar returns can be used to infer the gradient of refractivity structure near the ground [*Park and Fabry*, 2011; *Gerstoft et al.*, 2003b].

[6] Atmospheric ducts are more common in hot and humid regions of the world. The Persian Gulf, the Mediterranean and California coasts are examples of such regions with common formation of a ducting layer above the sea surface [*Yardim et al.*, 2009]. Surface based ducts appear on an annual average almost 25% of the time off the coast of South California and 50% in the Persian Gulf [*Patterson*, 1987]. While surface-based ducts appear less common than evaporation ducts, their effect is more prominent on the radar return [*Skolnik*, 2008]. They often manifest themselves in a radar plan position indicator (PPI) as clutter rings, see Figure 1d, or height errors in 3-D radars. The height error is due to the trapping of the lowest elevation beams near the surface instead of refracting upward as would be expected in a standard atmosphere.

[7] Figure 1b shows that a surface-based duct increases the radar range significantly inside the duct with respect to a weak evaporation duct (close to the standard atmosphere) by trapping the radar waves just above the ocean surface. Note that the electromagnetic energy is trapped inside the strong surface-based duct which results in an increase in the interaction of the electromagnetic waves with the sea surface. Figures 1c and 1d demonstrate the effect of atmospheric ducts on the radar clutter. The strong ducting case has distinct clutter rings around the radar. This complex clutter structure enables RFC to estimate the atmospheric conditions from the radar returns.

[8] Efforts by *Reilly and Dockery* [1990] and *Pappert et al.* [1992] to calculate sea reflections in ducting conditions inspired researchers to find the environmental refractivity profile from radar measurements, as opposed to the traditional way of using bulk sensor measurements. The atmospheric refractivity profile is often measured by direct

[1]Marine Physical Laboratory, Scripps Institute of Oceanography, University of California, San Diego, La Jolla, California, USA.
[2]Atmospheric Propagation Branch, Space and Naval Warfare Systems Center, San Diego, California, USA.

0048-6604/11/2011RS004818

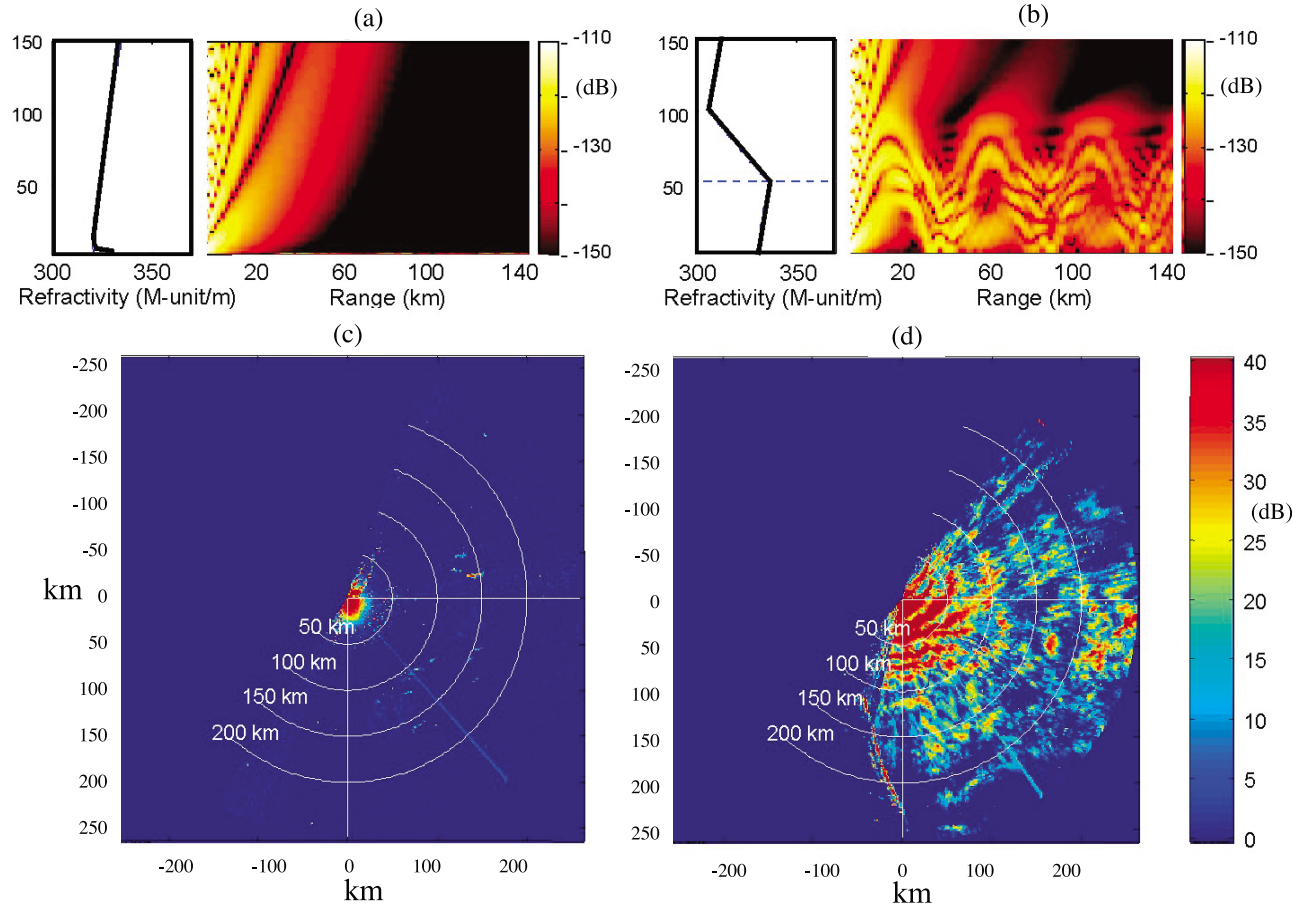

Figure 1. Propagation diagram of a (a) weak evaporation duct, (b) surface-based duct (high intensity: bright). Radar PPI screen showing clutter map (dB) during the 1998 SPANDAR experiment resulting from a (c) weak evaporation duct, (d) surface-based duct.

sensing of the environment. Rocketsondes and radiosondes typically are used for sampling of the atmospheric boundary layer [*Rowland et al.*, 1996], although they have limitations regarding mechanical issues and surface conditions [*Helvey*, 1983; *Mentes and Kaymaz*, 2007]. For characterization of the surface layer, "bulk" parameters such as pressure, air and sea surface temperature, humidity, and wind speed are measured at a single height, usually with sensors placed on a buoy or platform on the sea surface. These in-situ measurements are then used as inputs to thermodynamic "bulk" models to estimate the near-surface vertical refractivity profile using Monin-Obukhov similarity theory [*Jeske*, 1973; *Fairall et al.*, 1996; *Frederickson et al.*, 2000b].

[9] Initial remote sensing studies in the radar [*Richter*, 1995; *Rogers*, 1997] and climatology [*Haack and Burk*, 2001] communities have been directed toward a better estimation of the refractivity profile in the lower atmosphere, less than 500 m above the sea surface. *Hitney* [1992] demonstrated the capability to assess the base height of the trapping layer from measurements of UHF signal strengths. *Anderson* [1994] inferred vertical refractivity of the lower atmosphere based on ground-based measurements of global positioning system (GPS) signals, followed by *Lowry et al.* [2002] and *Lin et al.* [2011]. *Boyer et al.* [1996] estimated refractivity from radio measurements with diversity in frequency and height. *Rogers* [1997] used VHF/UHF measurements from the VOCAR 1993 experiment to invert for a three parameter (base height, M-deficit, and duct thickness) surface duct model. *Krolik and Tabrikian* [1997] used a maximum a posteriori (MAP) approach for inversions. They modeled the environment with a three element vector: two elements to describe the vertical structure and one to describe the range dependency of the profile. They later combined prior statistics of refractivity with point-to-point microwave propagation measurements to infer refractivity [*Tabrikian and Krolik*, 1999].

[10] *Von Engeln et al.* [2003] used low earth orbit GPS satellites to analyze the occurrence frequency and variation of land and sea ducts on a global scale, during a 10 day period in May 2001. LIDAR [*Wandinger*, 2005; *Willitsford and Philbrick*, 2005] has also been used to measure the vertical refractivity profile. However, its performance is limited by the background noise levels and high extinction (e.g., clouds) conditions.

[11] Weather radars and refractivity retrieval algorithms have been used to estimate moisture fields with high temporal and spatial resolution [*Fabry et al.*, 1997; *Weckwerth et al.*, 2005; *Roberts et al.*, 2008] with application in understanding

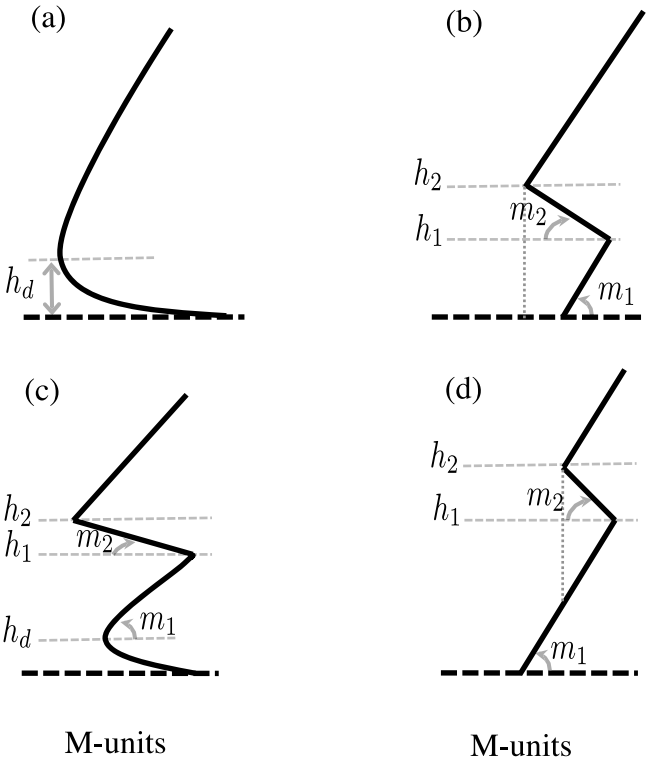

Figure 2. Parameters of simplified duct geometries: (a) evaporation duct, (b) surface-based duct, (c) surface-based duct with an evaporation layer, and (d) elevated duct.

thunderstorm initiation [*Wilson and Roberts*, 2006; *Wakimoto and Murphy*, 2009].

[12] RFC techniques use the radar return signals to estimate the ambient environment refractivity profile. There has been strong correlation between the retrieved refractivity profile using an S-band radar and in-situ measurements by instrumented aircrafts or radiosondes [*Rogers et al.*, 2000; *Gerstoft et al.*, 2003b; *Weckwerth et al.*, 2005]. RFC techniques make tracking of spatial and temporal changes in the environment possible [*Vasudevan et al.*, 2007; *Yardim et al.*, 2008; *Douvenot et al.*, 2010]. RFC inversions of the environmental profile have been reported at frequencies as low as VHF [*Rogers*, 1997], and as high as 5.6 GHz [*Barrios*, 2004].

[13] The development of RFC initially was inspired by the use of inverse methods in ocean acoustics which also is based on propagating signals in a waveguide. For a review of numerical modeling of the ocean waveguide consult *Jensen et al.* [2011]. For an introduction to the ocean acoustic inverse problem see *Dosso and Dettmer* [2011], and for sequential inverse methods in ocean acoustics see *Yardim et al.* [2011].

[14] The remainder of this paper is organized as follows: Section 2 introduces the marine ducts and their simplified mathematical models. Section 3 summarizes the clutter models used in previous studies and wave propagation approximations that model radio wave propagation efficiently. Section 4 summarizes the RFC research and inversion methods that have been used to infer the environmental refractivity parameters. Section 5 discusses the shortcomings of the current research and areas that require more attention in the future.

2. Marine Ducts

[15] One of the first reports of abnormal performance of radar systems in maritime environments was during World War II where British radars on the northwest coast of India commonly observed the coast of the Arabian peninsula 2700 km apart under monsoon conditions [*Kerr*, 1951]. Marine ducts are the result of heat transfer, moisture and the momentum of changes in the atmosphere [*Gossard*, 1981] and entail three general classes: evaporation, surface-based and elevated ducts.

[16] These ducts are characterized by a range and height dependent environmental refractivity index. Although a refractivity profile has a complex structure in nature, it can be approximated by a bilinear or trilinear function for surface-based ducts and by an exponential function for evaporation ducts in modeling wave propagation [*Dougherty and Hart*, 1979; *Rogers*, 1996; *Gerstoft et al.*, 2003b].

[17] The simplified atmospheric duct geometries used in most RFC works are shown in Figure 2. The modified refractive index M is defined as the part per million deviation of the refractive index from that of a vacuum:

$$M(z) \cdot 10^{-6} = n(z) - 1 + z/r_e, \tag{1}$$

which maps the refractivity index n at height z to a flattened earth approximation with earth radius r_e = 6370 km. The advantage of working with the modified refractive index is to transform a spherical propagation problem into a planar one. This transformation maps a spherically stratified medium over a spherical earth to a planar stratified medium above a flat earth. This transformation results in less than 1% error for ranges of less than $r_e/3$, independent of the wavelength [*Pekeris*, 1946]. However, this transformation to compute the height-gain function breaks down in centimeter wavelengths and elevation of more than 300 m. The error gets worse with increasing frequency [*Pekeris*, 1946].

2.1. Evaporation Ducts

[18] Existence of evaporation ducts was first suggested by *Katzin et al.* [1947]. Because of the difficulties in directly measuring the evaporation duct, various bulk models have been used to estimate the near-surface refractivity profile for several decades [*Jeske*, 1973; *Liu et al.*, 1979; *Paulus*, 1985; *Babin et al.*, 1997]. An evaporation duct model that assumes horizontally varying meteorological conditions has been suggested by *Greenaert* [2007]. Examples of such conditions are reported to frequently happen in the Persian Gulf [*Brooks et al.*, 1999]. One of the more widely accepted high fidelity evaporation duct models which has been used in various evaporation duct research studies is the model developed by the Naval Postgraduate School [*Frederickson et al.*, 2000a]. A heuristic 4-parameter model for range independent evaporation ducts that controls the duct height, M-deficit and slope has been suggested by *Zhang et al.* [2011b].

[19] The Paulus-Jeske (PJ) evaporation duct model is more commonly used operationally due to its empirical correction for spuriously stable conditions. The PJ model is based on the

air and sea surface temperatures, relative humidity, wind speed with sensor heights at 6 m and the assumption of a constant surface atmospheric pressure [*Jeske*, 1973; *Paulus*, 1985; *Babin et al.*, 1997]. For the neutral evaporation duct, where the empirical stability functions approach a constant, the PJ model is simplified to [*Rogers et al.*, 2000]:

$$M(z) = M_0 + c_0\left(z - h_d \ln\frac{z+z_0}{z_0}\right), \tag{2}$$

in which M_0 is the base refractivity, c_0 = 0.13 M-unit/m corresponding to the neutral refractivity profile as described by *Paulus* [1990], z_0 is the roughness factor taken as 1.5×10^{-4} m, and h_d is the duct height. The exact choice of M_0 (usually taken in the interval [310–360] M-units/m) does not affect the propagation pattern since it is the derivative of M that dictates wave propagation in the medium [*Hitney*, 1994; *Gerstoft et al.*, 2000].The assumption of neutral stability implies that the air and sea-surface temperature difference is nearly zero, and wind speed is no longer required. It was found by *Rogers and Paulus* [1996] that propagation estimates based on a neutral-stability bulk model performed well relative to other more sophisticated bulk models for the measurement sets under consideration. This is an important point as all RFC-estimated evaporation duct heights, and subsequently evaporation duct profiles given in (2), are based on neutral conditions.

2.2. Surface-Based Ducts

[20] Surface ducts typically are due to the advection of warm and dry coastal air to the sea. The trilinear approximation of the M-profile, as shown in Figure 2b, is represented by:

$$M(z) = M_0 + \begin{cases} m_1 z & z \le h_1 \\ m_1 h_1 + m_2(z - h_1) & h_1 \le z \le h_2 \\ m_1 h_1 + m_2(h_2 - h_1) + m_3(z - h_1 - h_2) & h_2 \le z \end{cases} \tag{3}$$

where m_3 = 0.118 M-units/m, consistent with the mean over the United States. Since profiles are upward refracting, clutter power is not very sensitive to m_3 [*Gerstoft et al.*, 2003b].

[21] A surface duct, schematically shown in Figure 2c, has also been used by *Gerstoft et al.* [2003b], and *Rogers et al.* [2005], which includes an evaporation duct layer beneath the trapping layer:

$$M(z) = M_0 + \begin{cases} M_1 + c_0\left(z - h_d \ln\frac{z+z_0}{z_0}\right) & z \le z_d \\ m_1 z & z_d \le z \le h_1 \\ m_1 h_1 - M_d \frac{z - h_1}{z_{\text{thick}}} & h_1 \le z \le h_2 \\ m_1 h_1 - M_d + m_3(z - h_2) & h_2 \le z \end{cases} \tag{4}$$

where c_0 = 0.13, m_1 is the slope in the mixed layer, m_3 = 0.118 M-units/m, h_1 is the trapping layer base height, and z_d is the evaporation duct layer height determined by:

$$z_d = \begin{cases} \frac{h_d}{1 - m_1/c_0} & 0 < \frac{1}{1 - m_1/c_0} < 2 \\ 2h_d & \text{Otherwise} \end{cases} \tag{5}$$

subject to $z_d < h_1$. $h_1 = 0$ simplifies (4) to a bilinear profile and $h_2 = 0$ implies standard atmosphere. z_{thick} is the thickness of the inversion layer, and $h_2 = h_1 + z_{\text{thick}}$. M_1 is determined by $M_1 = c_0 h_d \ln\frac{z_d + z_0}{z_0} + z_d(m_1 - c_0)$, and M_d is the M-deficit of the inversion layer. *Gerstoft et al.* [2003b] used an 11 parameter model for the environmental refractivity profile: five parameters for the vertical structure as in (4), and six to model the range variations of the profile. They assumed that the trapping layer height h_2 is range dependent and used principle components of h_2 as a Markov process with respect to range.

[22] Most of the RFC studies including works by *Gerstoft et al.* [2004], *Yardim et al.* [2007], and *Vasudevan et al.* [2007] have used a four parameter surface based duct.

[23] However, the frequency range of the validity of a trilinear approximation to the surface duct refractivity structure is arguable. As Figure 3 demonstrates, the trilinear approximation to complex refractivity profile structures gets worse for modeling wave propagation at higher frequencies. Propagation loss and clutter power of a measured profile and its trilinear approximation are shown in Figure 3. The profile is from the SPANDAR 1998 data set (Run 07, range 50 km) measured by an instrumented helicopter along the 150° azimuth shown in Figure 1 [*Rogers et al.*, 2000]. Figure 3a shows the trilinear approximation obtained by minimizing the l_2 norm of the difference of the approximated and real profiles given that the slope of the third line is fixed and equal to 0.12 M-units/m. Figure 3b shows the propagation loss of the measured profile with antenna height of 25 m, frequency of 3 GHz, beamwidth of 0.4° and wind speed of 5 m/s. The propagation loss is obtained from the Advanced Propagation Model [*Barrios*, 2002] which uses a parabolic equation code [*Barrios*, 1994]. The clutter power is obtained from a multiple angle clutter model (A. Karimian et al., Multiple grazing angle sea clutter modeling, submitted to *IEEE Transactions on Antennas and Propagation*, 2011, hereinafter referred to as A. Karimian et al., submitted manuscript, 2011a). Figures 3c and 3d show that the error of the trilinear approximation for a complicated structure increases with frequency. Here, the average absolute error of the propagation loss inside the duct increases from 4.9 dB at 3 GHz to 6.7 dB at 10 GHz. The absolute value of the clutter power difference due to the measured refractivity profile and its trilinear approximation increases from the average of 8.2 dB at 3 GHz to 13.3 dB at 10 GHz. However, experimental measured profiles show that the trilinear approximation is sufficient for most of the surface-based ducts, especially when propagation is to be modeled at 3 GHz and lower frequencies [*Gerstoft et al.*, 2003b; *Yardim et al.*, 2008].

[24] A wavelet representation of the conductivity profile was suggested in the similar inverse scattering problems arising in geophysical prospecting [*Miller and Willsky*, 1996a, 1996b]. Generalized Karhunen-Loeve transform [*Hua and Liu*, 1998] was used by *Kraut et al.* [2004] to find the tropospheric refractivity basis vectors of VOCAR 1993 profiles measured off the coast of California. Both of these approaches are capable of representing environmental profiles in more detail with additional complexity in inversions.

2.3. Elevated Ducts

[25] Elevated ducts, schematically shown in Figure 2d, are unstable atmospheric conditions that are primarily observed over the land but may also be formed across the seashore when cool air flows over a warmer sea [*Guinard et al.*,

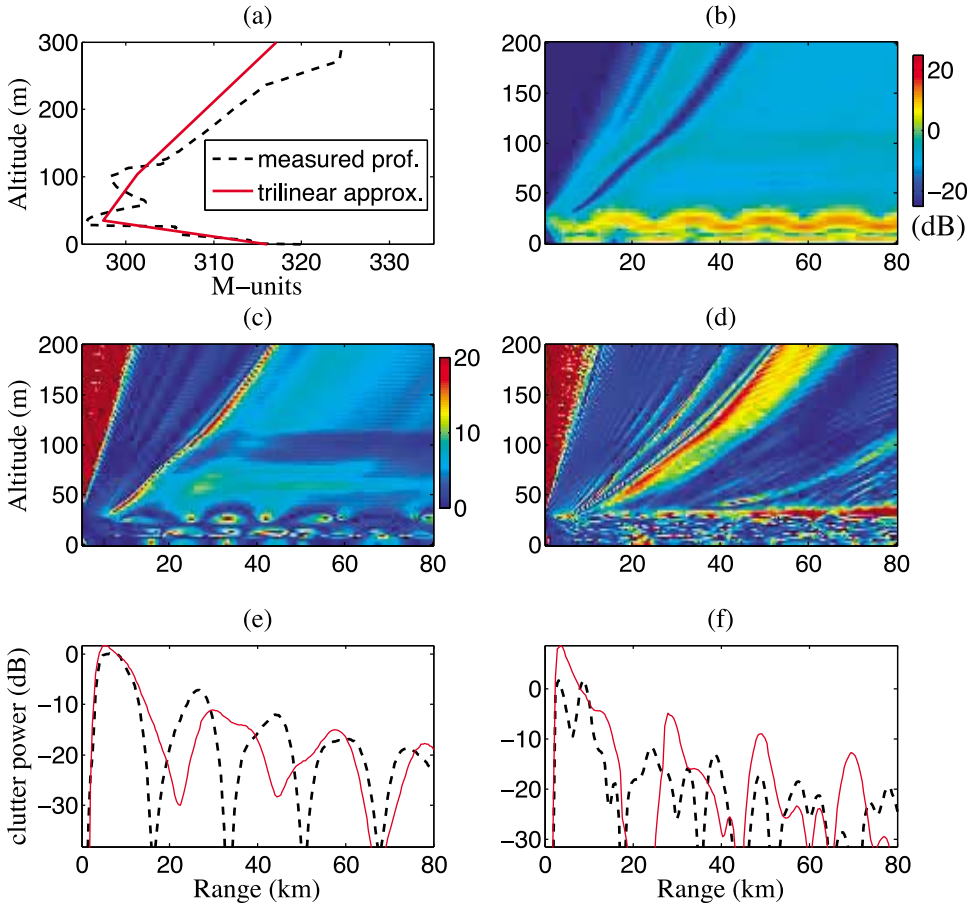

Figure 3. (a) A measured profile from the 1998 SPANDAR and its trilinear approximation. (b) Propagation loss (dB) of the measured profile at 3 GHz. Propagation loss difference of the measured profile and the trilinear approximation at (c) 3 GHz, and (d) 10 GHz. Clutter power comparison of the profile and its trilinear approximation at (e) 3 GHz, and (f) 10 GHz.

1964; *Gossard*, 1981; *Kukushkin*, 2004]. The effects from these types of ducts are not visible on a radar screen since radar beams get trapped in the elevated layer above the ocean level. Elevated ducts might be predicted from the nature of heat absorbing and radiating boundaries and the cloud cover [*Gossard*, 1981].

3. Electromagnetic Theory and Forward Modeling

[26] Given a refractivity structure **m** in a maritime environment, the expected clutter power is obtained as a function of radar and environmental parameters. Assuming that electromagnetic waves hit the surface at a single grazing angle at range r, the received radar power is [*Dockery*, 1990; *Skolnik*, 2008]:

$$P_r(r) = \frac{P_t G A_e \sigma F^4(r, \mathbf{m})}{(4\pi)^2 r^4 L}, \tag{6}$$

where P_t is the transmitter power, G the antenna gain, A_e the antenna effective aperture, σ the effective cross section of the scatterer, L the total assumed system losses, and F is the propagation factor at the sea surface. The pattern propagation factor F is defined as the ratio of the magnitude of the electric field at a given point under specified conditions to the magnitude of the electric field under free-space conditions [*Kerr*, 1951]: $F(r) = \frac{|E(r)|}{|E_{fs}(r)|}$. F is a function of range r and the refractivity structure **m** at each location. The antenna effective aperture is obtained as a function of the wavelength λ, $A_e = \frac{\lambda^2 G}{4\pi}$. The clutter cross section σ becomes $\sigma = A_c \sigma_0$ where σ_0 is the clutter cross section per unit area and A_c is the area of the radar cell [*Skolnik*, 2008]:

$$A_c = r\theta_B (c\tau/2) \sec(\theta(r, \mathbf{m})), \tag{7}$$

with θ_B the antenna pattern azimuthal beamwidth, c the propagation speed, τ the pulse width, and θ is the grazing angle which is a function of range and the environmental refractivity. From this point on, $F(r, \mathbf{m})$ and $\theta(r, \mathbf{m})$ are shown as F and θ for simplicity. Thus, the clutter power at the range r is obtained as:

$$P_c(r) = \frac{P_t G^2 \lambda^2 \theta_B c\tau \sigma_0 \sec(\theta) F^4}{2(4\pi r)^3 L}. \tag{8}$$

[27] The propagation factor F is calculated by numerical solutions to the wave propagation problem (section 3.1). The sea surface-reflectivity per unit area σ_0 is calculated

from semi-empirical models that fit the experimental measurements to a function of system parameters (section 3.2).

[28] The angle with which electromagnetic waves hit the ocean surface θ varies with range. However, the dependence of the clutter model on grazing angle has been neglected at far distances from the radar in [*Rogers et al.*, 2000, 2005; *Gerstoft et al.*, 2003b; *Kraut et al.*, 2004; *Yardim et al.*, 2006, 2008; *Vasudevan et al.*, 2007; *Wang et al.*, 2009; *Douvenot and Fabbro*, 2010; *Zhao et al.*, 2011]. The sec(θ) term also is a weak function of θ at low angles. Thus, normalization of the clutter power by the power at range r_0 yields the approximation:

$$\frac{P_c(r)}{P_c(r_o)} \simeq \left(\frac{r_o}{r}\right)^3 \frac{F^4(r)}{F^4(r_o)}. \tag{9}$$

[29] *Rogers et al.* [2000] considered the dependency of the sea-surface reflectivity with grazing angle in an evaporation duct and concluded that $\sigma_0 \propto \theta^0$ given that the clutter cells are far enough from the radar. There are similar surface reflectivity interpretations [e.g., *Douvenot et al.*, 2010] that also result in equation (9). *Rogers et al.* [2000] also investigated the existence of a minimum wind speed under which radar return is not reliable for duct height inversion. The minimum wind speed (usually less than is 2 m/s) depends on the radar parameters and sensitivity.

[30] To overcome the problem of uncertainty of σ_0, geometrical ray tracing and rank correlation was used by *Barrios* [2004] for inversion of surface-based ducts.

[31] The assumption that there is a single grazing angle θ at each range is not always valid, especially in strong surface-based ducts where multiple electromagnetic waves with different angles hit the surface at each location. A. Karimian et al. (submitted manuscript, 2011a) suggested a clutter model that depends on all grazing angles proportional to their relative powers:

$$P_c(r) = \frac{\alpha_c(r)F^4(r)}{\int_\theta \gamma(\theta)d\theta} \int_\theta \frac{\sigma_{0,GIT}(\theta)\sec(\theta)\gamma(\theta)}{F^4_{std}(\theta)} d\theta, \tag{10}$$

where $\alpha_c(r) = \frac{P_t G^2 \lambda^2 \theta_B c\tau}{2(4\pi r)^3 L}$ includes all grazing angle independent terms, $\sigma_{0,GIT}$ is the sea surface reflectivity from the GIT model (discussed in Section 3.2), $\gamma(\theta)$ is the relative energy of incident wavefronts at each grazing angle obtained from a curved wave beamformer, and $F_{std}(\theta)$ is the propagation factor of a standard atmosphere at a range with the same grazing angle. An analysis of the performance of different clutter models in RFC inversions is provided by A. Karimian et al. (Estimation of refractivity using a multiple angle clutter model, submitted to *Radio Science*, 2011, hereinafter referred to as A. Karimian et al., submitted manuscript, 2011b).

3.1. Wave Propagation Modeling

[32] From the early days of wave propagation modeling, a divergence arose due to the distinct differences in applications emphasizing environmental effects over terrain versus over the oceans. Due to the advances in computer processing as well as innovative mathematical techniques for numerically intensive problem solving, the most popular techniques for Radio Frequency (RF) propagation modeling have converged such that these same methods are well suited for both land and water propagation paths. Since the emphasis of this paper is on the estimation of refractive conditions over the ocean, this section will describe only those RF propagation modeling techniques and algorithms as they pertain to modeling anomalous propagation effects on over-water paths.

[33] One of the first radio wave propagation models that took into account the effects of both evaporation ducts and surface-based ducts was based on the techniques described by *Kerr* [1951] and *Blake* [1980]. The model determines the coherent sum of the direct and surface-reflected fields within the optical interference region, also accounting for divergence and non-perfect reflection by use of a modified Fresnel reflection coefficient [*Hitney and Richter*, 1976]. Modeling refractive effects is limited since within this region, the use of an effective earth radius factor is employed to account for non-standard conditions. For diffraction effects beyond the radio horizon, ducting effects are based on a single mode model where an empirical fit to waveguide solutions are used to modify Kerr's standard diffraction method [*Hitney*, 1994].

[34] For modeling of height-varying refractive conditions, waveguide models offer a much higher fidelity solution and have been in use since the early 1900s [*Budden*, 1961]. Waveguide models employ normal mode theory and are well suited when refractive conditions do not change along the path. Due to the high computational requirements for mode searches, another caveat is that normal mode models are typically used beyond the radio horizon where far fewer modes are needed for a solution [*Pappert et al.*, 1992; *Hitney*, 1994].

[35] One of the more popular techniques for RF propagation modeling is the parabolic equation (PE) method, also known as the paraxial approximation method. Originally used by *Leontovich and Fock* [1946], the PE method allows for propagation conditions to vary in both height and range. However, the PE method was not in practical use until *Hardin and Tappert* [1973] developed a technique called the split-step Fourier (SSF) method, initially applied to underwater acoustic propagation. The SSF method took advantage of fast Fourier transforms that led to extremely efficient numerical solutions of the PE. *Ko et al.* [1983] and *Skura et al.* [1990] modified the underwater acoustic SSF PE to model radio wave propagation in the troposphere. Since that time many improvements and mathematical techniques have been introduced in the SSF PE algorithm for applications to RF propagation in the troposphere. For an excellent treatise on the development of many of these techniques, the reader is referred to work by *Levy* [2000].

[36] Due to its efficiency and accuracy the SSF PE algorithm is now widely used in many radio wave propagation models, including the model used here to obtain results presented in this paper. A general description of the SSF PE algorithm is given in the following, with more details provided on specific implementation of the model used here. Applying the simple assumption of a slowly varying medium, Maxwell's equations can be reduced to the scalar two-dimensional (Cartesian) elliptical Helmholtz equation:

$$\frac{\partial^2 \psi(x,z)}{\partial x^2} + \frac{\partial^2 \psi(x,z)}{\partial z^2} + k_0^2 n^2 \psi(x,z) = 0, \tag{11}$$

where $\psi(x, z)$ is a function of the electric or magnetic field, depending on the polarization of the radiated field; and n is the refractive index of the medium (implicitly also a function of x and z). The usual starting point for the derivation of the PE is substituting the function $\psi(x, z) = e^{jk_0x}u(x, z)$ in (11), then factor the result into, respectively, forward and backward pseudo-differential equations:

$$\frac{\partial u(x,z)}{\partial x} + jk_0\left[1 - \sqrt{\frac{1}{k_0^2}\frac{\partial^2}{\partial z^2} + n^2}\right]u(x,z) = 0, \tag{12}$$

$$\frac{\partial u(x,z)}{\partial x} + jk_0\left[1 + \sqrt{\frac{1}{k_0^2}\frac{\partial^2}{\partial z^2} + n^2}\right]u(x,z) = 0. \tag{13}$$

[37] This substitution effectively removes the rapid phase variation in ψ, leaving $u(x, z)$ a slowly varying function in range. In most PE models used for long range radio wave tropospheric propagation, only the forward propagating term (12) is solved, and the backward propagating term is ignored.

[38] Initial PE algorithms incorporated simple approximations to (12), resulting in the standard PE (SPE). The limitation with using the SPE is that it is a narrow-angle approximation and leads to larger errors when propagating at large angles, typically greater than 10° for microwave frequencies. *Feit and Fleck* [1978] developed the wide-angle PE (WAPE) for propagation within optical fibers, by using an alternative approximation of the square-root operator. Later, *Thomson and Chapman* [1983] quantified the error associated with the use of various approximations to the square-root operator, concluding that the WAPE propagator developed by Feit and Fleck was a substantial improvement in reducing phase errors at large propagation angles necessary for their work in underwater acoustic propagation. More recently, *Kuttler* [1999] analyzed the differences between the SPE and WAPE and offered yet a further improvement for the WAPE and wide-angle sources.

[39] The Leontovich surface impedance boundary condition must then be applied to obtain a solution for the WAPE:

$$\left.\frac{\partial u}{\partial z}\right|_{z=0} + \alpha u|_{z=0} = 0, \tag{14}$$

where the complex α is given by

$$\alpha_{h,v} = jk_0 \sin\theta\left[\frac{1 - \Gamma_{h,v}}{1 + \Gamma_{h,v}}\right]. \tag{15}$$

Here, θ is the grazing angle of the radiated field at the surface, Γ is the Fresnel reflection coefficient - also dependent on the grazing angle, and the subscripts h and v refer to horizontal and vertical polarization respectively. The discrete mixed Fourier transform (DMFT) formulation provided by *Dockery and Kuttler* [1996] implements the impedance boundary condition and derives the new split-step solution entirely in the discrete domain. The DMFT method has the added advantage that it retains numerical efficiency due to requiring only sine transforms. Further refinement of the DMFT was presented by *Kuttler and Janaswamy* [2002] where they applied various difference formulations for (14) to arrive at an improved DMFT algorithm, reducing much of the numerical instabilities associated with the quantity $\alpha_{h,v}$ when $Re(\alpha_{h,v})$ approaches zero.

[40] The propagation model used for the results presented in this paper implements the WAPE and the DMFT algorithm as described by *Kuttler* [1999], *Dockery and Kuttler* [1996], and *Kuttler and Janaswamy* [2002] and is called the Advanced Propagation Model (APM). The handling of range-varying vertical refractive profiles is described by *Barrios* [1992] and a general description of the APM is provided by *Barrios* [2003].

[41] Pertinent to the RFC methodology is the accuracy of the forward scattered field, which is subsequently dependent on how $\alpha_{h,v}$ is modeled. Typically, the boundary condition is modeled such that a constant impedance is assumed within each range step, dependent on a single grazing angle associated with the dominant mode of propagation for the specified refractive environment. We apply the Kirchoff approximation and model the sea surface boundary by determining an effective impedance described by a reduction, ρ, to the smooth surface Fresnel reflection coefficient, Γ_0, based on the Miller-Brown-Vegh (MBV) model [*Miller et al.*, 1984]:

$$\Gamma_{h,v} = \rho\Gamma_{0h,v} \tag{16}$$

$$\rho = e^{-2(2\pi\gamma)^2} I_0\left[2(2\pi\gamma)^2\right] \tag{17}$$

$$\gamma = \frac{h_w \sin\theta}{\lambda} \tag{18}$$

[42] I_0 is the modified Bessel function of the first kind, and h_w is the RMS wave height from the Phillips ocean wave spectrum [*Phillips*, 1985]:

$$h_w = 0.0051 v_w^2, \tag{19}$$

where v_w is the wind speed in m/s. Within APM, ρ is approximated according to the *International Telecommunications Union* [1990] by the expression

$$\rho = \frac{1}{\sqrt{3.2\chi - 2 + \sqrt{(3.2\chi)^2 - 7\chi + 9}}}, \tag{20}$$

$$\chi = \frac{1}{2}\gamma^2. \tag{21}$$

[43] Next is to determine the grazing angle at each PE range step to compute the effective reflection coefficient and subsequent impedance. Grazing angles at the sea surface can easily be found using a geometric ray trace based on small angle approximations to Snell's law [*Dockery et al.*, 2007]. The caveat is that for surface-based ducting conditions, there will be multiple grazing angles within a given range interval/step, as shown in Figure 4. Figure 4a shows the refractivity profile of a 300 m surface-based duct, and the corresponding grazing angles are shown in Figure 4b. Notice that beyond the skip zone, at ranges beyond 80 km, there are multiple grazing angles (i.e., multiple modes) present within a given

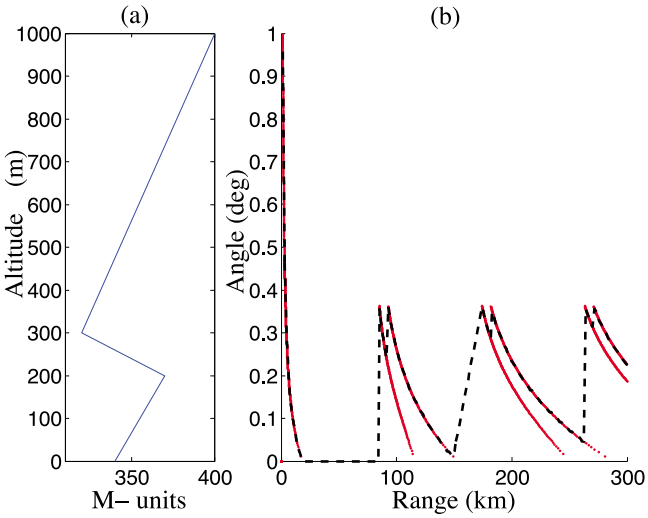

Figure 4. (a) Refractivity profile of surface-based duct used for (b) determination of grazing angles by ray trace (solid) and final maximum angles (dashed lines) used for computing $\alpha_{h,v}$.

range interval. The challenge is determining the proper grazing angle associated with the dominant mode of propagation at a particular range. Geometric ray tracing techniques offer no further information, therefore, spectral estimation techniques have also been used [*Dockery and Kuttler*, 1996; *Schmidt*, 1986; *Barrios*, 2003] in combination with geometric ray trace methods to obtain the appropriate angle at a given range particularly useful in complex environments where the propagation path is a combination of sea, land, and a range-dependent atmosphere.

[44] Of course, one of the caveats of modeling the impedance in this way is that for surface-based ducting environments it ignores the many, equally dominant, modes propagating within the duct at multiple grazing angles within a range step. The advantage of using the MBV method to modify the surface impedance is that it is easy to implement and for the most part has been shown to perform very well for range-independent evaporation duct environments where the incident field can be described, to a very good approximation, by a single grazing angle beyond the interference region [*Anderson*, 1995; *Rogers et al.*, 2000].

[45] A more rigorous, albeit conventional, approach has been provided by *Janaswamy* [2001] to model a non-constant impedance that directly takes into account effects of the angle-dependent reflection coefficient present at all grazing angles. However, in keeping with the more numerically efficient SSF PE approach, and considering the design toward operational applications, the maximum grazing angle (shown by the dashed line in Figure 4b) is used in computing $\alpha_{h,v}$ to model rough surface effects. This results in maximum, or worst-case, clutter values and will in general over-estimate sea clutter.

[46] Finally, a recent approach to more accurately model the various field strengths at the surface, and subsequently, clutter power described by multiple grazing angles, has been provided by A. Karimian et al. (submitted manuscript, 2011a) that takes all grazing angles and their relative powers at each range-step into account.

[47] For the RFC application, the propagation factor, F, in the clutter equations (8–10) is a function of the complex PE field and the range (note that range is shown by r in the clutter equations and by x in this section, since Maxwell's equations are solved in Cartesian coordinates):

$$F = |u(x, z_{\text{eff}})|\sqrt{x}, \tag{22}$$

where z_{eff} is the effective scattering height, taken as 0.6 times the mean wave height [*Reilly and Dockery*, 1990], or approximately 1 m above the ocean for most situations [*Rogers et al.*, 2000; *Barrios*, 2003]. Theoretically, F should be computed from the incident field at the sea surface. However, PE approximations yield the propagation factor due to the total field which is close to zero at the sea surface and high frequencies. *Konstanzer et al.* [2000] showed that the clutter power using the total field propagation factor at the effective scattering height is proportional to the clutter power using the incident propagation factor.

3.2. Sea Surface Reflectivity Models

[48] Proper characterization of the quantity $\sigma_0 F^4$ in (8) is key to providing reasonable clutter predictions to perform RFC. The difficulty is that the surface reflectivity is implicitly dependent on the forward propagation effects defined by F. They are inherently coupled yet these two quantities are commonly treated separately to get an estimate of the return clutter. Most sea surface reflectivity models, therefore, are semi-empirical and are based on site-specific propagation data, typically with no corresponding meteorological measurements.

[49] There are several semi-empirical models for the average sea surface reflectivity per unit area that fit the experimental sea clutter data to a function of radar frequency, grazing angle, beam width, wind speed, radar look direction with respect to the wind, and polarization. This quantity, represented by σ_0, is also referred to as the normalized radar reflectivity [*Nathanson et al.*, 1991].

[50] A hybrid model by *Barton* [1988] and the Georgia Institute of Technology (GIT) model [*Horst et al.*, 1978] are among the classic sea surface reflectivity models for low grazing angles that are valid in the S and X-band frequencies. A comparison of the GIT, Technology Services Corp. (TSC) [*Fletcher*, 1978], and Barton (BAR) reflectivity models at 3 GHz is shown in Figure 5a [*Reilly and Dockery*, 1990]. A similar comparison at 9.3 GHz with the additional Sittrop (SIT) [*Sittrop*, 1977] model is shown in Figure 5b. Notice that the TSC, BAR, and SIT models show similar dependence of σ_0 on grazing angle, whereas the GIT model exhibits higher attenuation at lower grazing angles. Lower grazing angles imply the region near the radio horizon subject to diffraction effects. The increased attenuation shown by the GIT model as a function of decreasing grazing angle is indicative of standard diffraction effects, and it is for this reason the GIT model has been more widely used. That is, the GIT reflectivity can be assumed to be representative of σ_0 under standard atmosphere conditions.

[51] *Reilly and Dockery* [1990] modified the GIT model to consider ducting effects on the radar backscatter by dividing σ_0 by the standard atmosphere propagation factor and multiplying by the propagation factor of the desired conditions [*Dockery*, 1990].

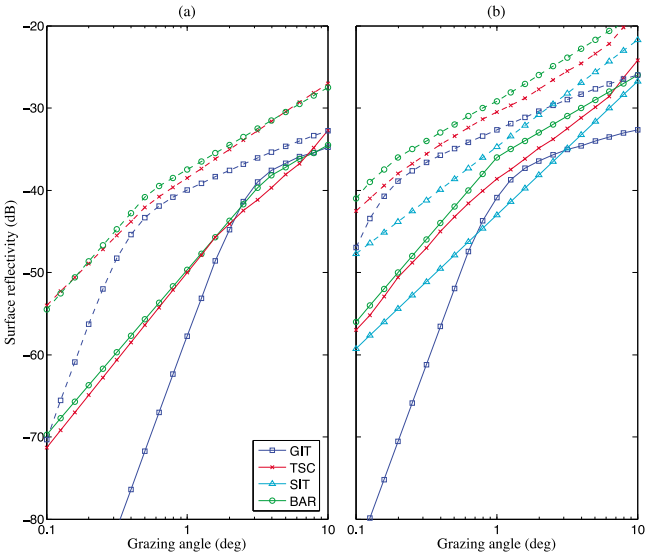

Figure 5. Reflectivity versus grazing angle for several sea surface reflectivity models at (a) 3 GHz, and (b) 9.3 GHz for sea states $S = 2$ (solid) and $S = 5$ (dashed) [*Reilly and Dockery*, 1990].

[52] Normalized mean sea backscattering coefficient σ_0 for grazing angles of 0.1 to 60° and frequencies of 0.5 to 35 GHz are tabulated by *Nathanson et al.* [1991] based on almost 60 experiments. A model to fit the aforementioned data set for grazing angles less than 10° and frequencies up to 35 GHz is provided by *Gregers-Hansen and Mital* [2009]. Modeling the sea surface reflectivity suitable for RFC applications remains an active field of research.

[53] Calculation of the grazing angle is the key to the calculation of radar backscatter. A hybrid of ray tracing and plane wave beamforming has been suggested in the works of *Dockery and Kuttler* [1996], *Barrios* [2003], and *Dockery et al.* [2007] to find the angle of arrival based on the propagation conditions. A. Karimian et al. (submitted manuscript, 2011a) suggested a curved wave beamformer that depends on the refractivity profile at each location.

4. Inverse Problem Framework

[54] The radar clutter depends on the two way propagation loss from the transmitter to the range cell. The loss in turn depends on the environmental refractivity profile through which the wave is propagated. The expected clutter power of each candidate profile is computed and an objective function Φ that quantifies the difference between the observed, $\mathbf{P}_o$, and the simulated clutter power, $\mathbf{P}_s(\mathbf{m})$, is formed. $\mathbf{P}_o$ and $\mathbf{P}_s$ are the vectors of clutter power over the radar range. The candidate profile that yields the minimum difference is declared as the best match.

$$\hat{\mathbf{m}} = \underset{\mathbf{m}}{\operatorname{argmin}}\, \Phi(\mathbf{P}_o, \mathbf{P}_s(\mathbf{m})). \tag{23}$$

[55] The simulated clutter is a function of the propagation factor F, as seen in (6). F in turn, is a function of the environmental profile m. Using an l_2 norm as the objective function Φ yields:

$$\Phi = \|\mathbf{P}_o - \mathbf{P}_s(\mathbf{m})\|^2, \tag{24}$$

which is also the negative log likelihood function under the Gaussian noise assumption. Minimizing equation (23) over the refractivity profile $\mathbf{m}$ requires an efficient numerical search for the optimum values.

[56] There have been several approaches to estimate the refractivity parameters from the observed clutter including: a matched-field processing approach toward inversion [*Gerstoft et al.*, 2000], a genetic algorithm [*Gerstoft et al.*, 2003b], a Markov-chain Monte Carlo sampling approach to estimate the uncertainties of the inverted parameters [*Yardim et al.*, 2006], Markov state-space model for microwave propagation [*Vasudevan et al.*, 2007], Kalman and particle filters [*Yardim et al.*, 2008], support vector machines [*Douvenot et al.*, 2008], particle swarm optimization [*Wang et al.*, 2009], a Bayesian approach with meteorological prior [*Yardim et al.*, 2009], an improved best fit approach [*Douvenot and Fabbro*, 2010; *Douvenot et al.*, 2010] and a range adaptive objective function [*Zhang et al.*, 2011a].

[57] *Gingras et al.* [1997] suggested a matched-field processing approach for source localization and inversion for environmental parameters which was based on plotting ambiguity surfaces of unknown variables. *Gerstoft et al.* [2000] showed successful application of the matched-field processing technique to invert for surface-based duct parameters. They also showed that it was not possible to invert for elevated duct parameters using single surface measurements.

[58] Most of the previous RFC studies inverted the clutter power for the refractivity structure in a short range interval assuming changes in the refractivity profile to be negligible. *Gerstoft et al.* [2003b] inverted for a range-dependent profile by considering range-dependent parameters. *Vasudevan et al.* [2007] used a Markov chain model on the propagation state-space [*Rabiner*, 1989] to consider a range dependent profile. The latter approach reduces the complexity of inversions based on the number of unknown profiles with the added advantage of correcting inverted profile of shorter ranges efficiently by considering clutter power from longer ranges.

4.1. Likelihood Function

[59] The relationship between the observed complex-valued radar I and Q components of the field $\mathbf{u}_{I,o}$ and $\mathbf{u}_{Q,o}$ over N_r range bins and the predicted field $\mathbf{u}_{I,s}$ and $\mathbf{u}_{Q,s}$ is described by the model:

$$\mathbf{u}_{I,o} = \sqrt{\mathbf{n}_1}\mathbf{u}_{I,s}(\mathbf{m})e^{j\phi_1} + \mathbf{n}_2 e^{j\phi_2} \tag{25}$$

$$\mathbf{u}_{Q,o} = \sqrt{\mathbf{n}_1}\mathbf{u}_{Q,s}(\mathbf{m})e^{j\phi_1} + \mathbf{n}_2 e^{j\phi'_2} \tag{26}$$

where $\mathbf{n}_1$ is the multiplicative random variable in the modeled electric field due to a variable sea surface reflectivity. *Yardim et al.* [2009] considered different probability distributions for the random variable $\mathbf{n}_1$ including lognormal, K-distribution and Rayleigh. Here, a lognormal distribution is assumed for each element of the vector $\mathbf{n}_1$. Noise in the receiver, $\mathbf{n}_2$ and $\mathbf{n}'_2$, are modeled by Gaussian distributions. ϕ_1, ϕ_2, ϕ'_2 are

the random phase components of the complex random variable with uniform distributions:

$$\{\log n_1\}_1^N, \sim \mathcal{G}(0, \sigma_1^2) \tag{27}$$

$$\{n_2\}_1^N, \{n_2'\}_1^N \sim \mathcal{G}(0, \sigma_2^2) \tag{28}$$

$$\{\phi_1\}_1^N, \{\phi_2\}_1^N, \{\phi_2'\}_1^N \sim \mathcal{U}(0, \pi) \tag{29}$$

[60] The radar output power is obtained by:

$$\Pi = |\mathbf{u}_I|^2 + |\mathbf{u}_Q|^2. \tag{30}$$

Thus, the observed and simulated clutter power are related by:

$$\Pi_o = \mathbf{n}_1 \Pi_s(\mathbf{m}) + \mathbf{n}_r \tag{31}$$

$$\{\log \mathbf{n}_1\}_1^N \sim \mathcal{G}(0, \sigma_1^2) \tag{32}$$

$$\{\mathbf{n}_r\}_1^N \sim \chi^2 \tag{33}$$

where $\mathbf{n}_1$ is the multiplicative noise with a lognormal distribution, and $\mathbf{n}_r$ is the additive receiver noise with a χ^2 distribution and 2 degrees of freedom. Working in the high CNR (clutter to noise ratio) regime, the $\mathbf{n}_r$ term can be neglected. Thus, the modeled power in the logarithmic domain is obtained as:

$$\mathbf{P}_o = \mathbf{P}_s(\mathbf{m}) + \mathbf{n} \tag{34}$$

$$\{\mathbf{n}\}_1^N \sim \mathcal{G}(0, \sigma^2), \tag{35}$$

where, $\mathbf{P}_o$ and $\mathbf{P}_s(\mathbf{m})$ are vectors of the observed and simulated clutter power of the profile $\mathbf{m}$ in dB, and $\mathbf{n} = 10 \log \mathbf{n}_1$.

[61] More than one source of clutter power observations can be used in an inversion. These sources can include the clutter power at different frequencies, different radar elevation angles, or different snapshots with similar conditions where $\mathbf{P}_{n,o}$ corresponds to the nth source of the observed clutter power. Given N different sources with uncorrelated noise power ν_n, the maximum likelihood function becomes ($|\mathbf{x}| = (|x_1|, |x_2|, .)$ and $\|\mathbf{x}\|^2 = \sum_i |x_i|^2$):

$$\mathcal{L}(\mathbf{m}) = \prod_{n=1}^{N} (\pi \nu_n)^{-N_r} \exp\left[-\frac{\left\| \mathbf{P}_{o,n} - \mathbf{P}_{s,n}(\mathbf{m}) \right\|^2}{\nu_n} \right]. \tag{36}$$

[62] Assuming that the noise power $\{\nu_n\}_{n=1.N}$ is constant across different observations, the negative log likelihood function is simplified to

$$\Phi(\mathbf{m}) = -\log \mathcal{L}(\mathbf{m}) \propto \sum_{n=1}^{N} \left\| \mathbf{P}_{o,n} - \mathbf{P}_{s,n}(\mathbf{m}) \right\|^2. \tag{37}$$

[63] The maximum likelihood estimate $\hat{\mathbf{m}}$ for $\mathbf{m}$ is obtained by minimizing (37) over the model parameter vector $\mathbf{m}$, which is similar to (23).

4.2. An Inversion Example

[64] A set of refractivity profile measurements and radar returns was recorded at Wallops Island, Virginia, April 1998 [*Rogers et al.*, 2000; *Gerstoft et al.*, 2003b]. Clutter signals were measured using the Space Range Radar (SPANDAR) with operational frequency of 2.84 GHz, horizontal beamwidth of 0.4°, elevation angle of 0, antenna height of 30.78 m, and vertical polarization. The refractivity profiles of the environment were recorded using an instrumented helicopter provided by the Johns Hopkins University Applied Physics Laboratory. The helicopter flew in and out along the 150° radial from a point 4 km due east of the SPANDAR in a saw-tooth pattern with each transect lasting 30 min.

[65] The range-dependent refractivity profile measured by the helicopter is shown in Figure 6a. This profile corresponds to the measurement on April 2, 1998 from 13:19:14 to 13:49:00 (Run 07). The spatial variation of the M-profile is small in the 0–45 km range. Thus, RFC results of the corresponding clutter observations are compared to the average of the measured M-profiles in that range interval. Note that although the experimental measurements are from a range-dependent refractivity profile, inversions are based on a range-independent profile.

[66] Recorded clutter power of the SPANDAR between azimuth 142–166° is used to estimate the trilinear function representing a surface-based duct since the clutter pattern (Figure 1d) is rather stationary in this interval. The probability distribution of the refractivity profile from all inversion results is obtained and the maximum a posterior (MAP) solution of this distribution is found to be the refractivity profile that fits all data. Only the first 60 km of the radar clutter is used to invert for the refractivity profile to maintain a high CNR and to avoid high spatial variations of refractivity with range. A multiple angle clutter model based on curved wave beamforming (A. Karimian et al., submitted manuscript, 2011a) is used to calculate the clutter power, and APM [*Barrios*, 2003] is used to calculate the electric field and propagation loss. Figure 6 shows the inverted profiles obtained from clutter power observed along the 150° azimuth, the helicopter measured refractivity along the 150° azimuth and the span of inverted profiles using clutter power along 142–166°.

[67] Figure 7 shows the propagation loss using the inverted profile from Figure 6b and a standard atmosphere. Surface-based ducting conditions result in the extended range of the radar and radar fades in unexpected locations assuming a standard atmosphere. Radar parameters in this figure are identical to those of the SPANDAR.

4.3. Bayesian Approach

[68] One important motivation behind estimation of the refractivity structure in the environment is to predict the radar performance in non-standard atmospheric conditions. This requires the statistical properties of the parameters-of-interest such as the propagation loss which can be computed from the statistical properties of the atmospheric refractivity. The unknown environmental parameters are taken as random variables with corresponding one-dimensional (1-D) probability density functions (pdfs) and an n-dimensional joint pdf.

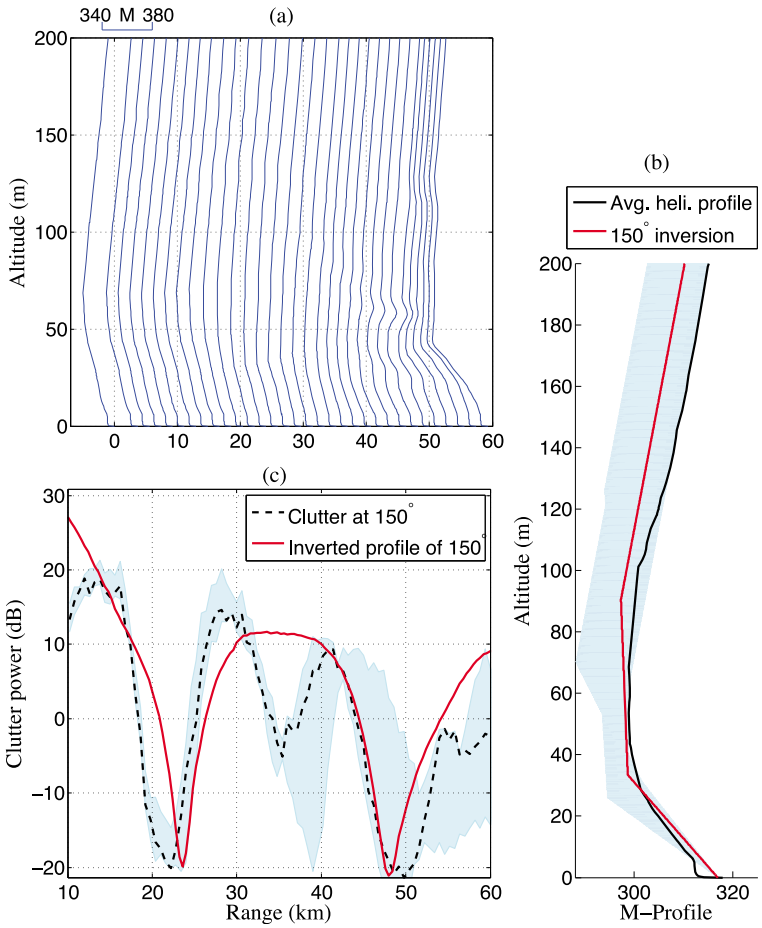

Figure 6. (a) Range-dependent refractivity profile recorded by an instrumented helicopter along the 150° azimuth. (b) Average of the first 45 km of the measured profile compared to the inverted profiles of 150° clutter (solid) and the MAP profile of 142–166° (shaded). (c) Observed and modeled clutter power of the inverted profile.

This probability function can be defined as the probability of the model vector $\mathbf{m}$ given the observed clutter power $\mathbf{P}_o$, $p(\mathbf{m}|\mathbf{P}_o)$, and it is called the posterior pdf (PPD). The profile $\mathbf{m}$ with the highest probability is referred to as the maximum a posteriori (MAP) solution. The posterior means, variances, and marginal probability distributions can be found by integrating over this PPD:

$$\mu_i = \int \dots \int_{\mathbf{m}'} m_i' p(\mathbf{m}'|\mathbf{P}_o) \mathrm{d}\mathbf{m}', \tag{38}$$

$$\sigma_i^2 = \int \dots \int_{\mathbf{m}'} (m_i' - \mu_i)^2 p(\mathbf{m}'|\mathbf{P}_o) \mathrm{d}\mathbf{m}', \tag{39}$$

$$p(m_i|\mathbf{P}_o) = \int \dots \int_{\mathbf{m}'} \delta(m_i' - m_i) p(\mathbf{m}'|\mathbf{P}_o) \mathrm{d}\mathbf{m}'. \tag{40}$$

[69] The posterior density of any specific environmental parameter can be obtained by marginalizing the n-dimensional PPD as given in (40) [*Kay*, 1993]. *Gerstoft et al.* [2004] used importance sampling (IS) [*MacKay*, 2003] to compute the necessary multidimensional integrals needed to map the environmental uncertainty into propagation loss uncertainty. IS produces unbiased distributions of the desired variables, however, the variance of the estimates depend heavily on the importance density used in IS. Another problem with IS is the slow rate of convergence for the numerical computation of the integrals. *Gerstoft et al.* [2004] also compared IS to using just the 1-D marginals of refractivity parameters to compute the PDF of propagation loss. As long as the interparameter correlations are negligible, using marginals is computationally more efficient than IS. They later showed that lowering the peak clutter to noise ratio broadens the a posteriori distribution of the propagation loss [*Rogers et al.*, 2005].

[70] The error in IS is minimized when samples are drawn from the posterior distribution of the environmental parameters $p(\mathbf{m}|\mathbf{P}_o)$. Sampling from the posterior requires a Markov chain Monte Carlo (MCMC) class sampler [*Ó Ruanaidh and Fitzgerald*, 1996; *MacKay*, 2003] such as the Metropolis-Hastings (MH) [*Metropolis et al.*, 1953] and the Gibbs samplers [*Geman and Geman*, 1984]. MCMC methods are guaranteed to asymptotically converge to the true parameter distribution at a high computational cost. *Yardim et al.* [2006] used a MH sampler to find the a posteriori distribution for the environmental model parameters and used the MH sampler output to map the environmental uncertainty into the propagation loss domain.

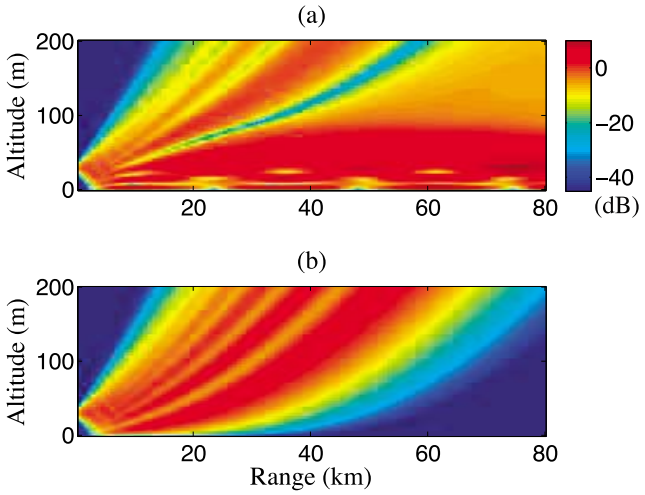

Figure 7. Propagation loss: (a) MAP estimate of the refractivity profile given the clutter power at 150° azimuth of SPANDAR Run 07, and (b) standard atmosphere.

[71] *Yardim et al.* [2007] introduced a hybrid genetic algorithms (GA)-MCMC method to estimate the posterior probability faster than MCMC which does not suffer from the bias of histograms obtained from the GA. The hybrid GA-MCMC approximates the posterior distribution faster than an MCMC by first performing a GA inversion, discretizing the environmental parameter domain using the GA samples via Voronoi decomposition and the nearest neighborhood method [*Sambridge*, 1999a, 1999b], and finally applying a fast Gibbs sampler over this discrete space. The posterior distribution can be found using the Bayes rule:

$$p(\mathbf{m}|\mathbf{P}_o) = \frac{p(\mathbf{m})\mathcal{L}(\mathbf{m})}{p(\mathbf{P}_o)} \propto p(\mathbf{m})\mathcal{L}(\mathbf{m}), \tag{41}$$

with

$$p(\mathbf{P}_o) = \int_{\mathbf{m}} p(\mathbf{P}_o|\mathbf{m})p(\mathbf{m})\mathrm{d}\mathbf{m}. \tag{42}$$

[72] The likelihood function $\mathcal{L}(\mathbf{m})$ is the same as in (36), assuming a zero-mean Gaussian distribution for the error. The prior $p(\mathbf{m})$ represents *a priori* knowledge about the environmental parameters $\mathbf{m}$, which might be from the meteorological statistics [*Yardim et al.*, 2009] or from the result of previous inversions [*Yardim et al.*, 2008; *Douvenot et al.*, 2010]. A non-informative or flat prior assumption reduces (42) to:

$$p(\mathbf{m}|\mathbf{P}_o) \propto \mathcal{L}(\mathbf{m}), \tag{43}$$

which has been discussed in section 4.1. Figure 8 is adopted from [*Yardim et al.*, 2006] which shows the highest posterior

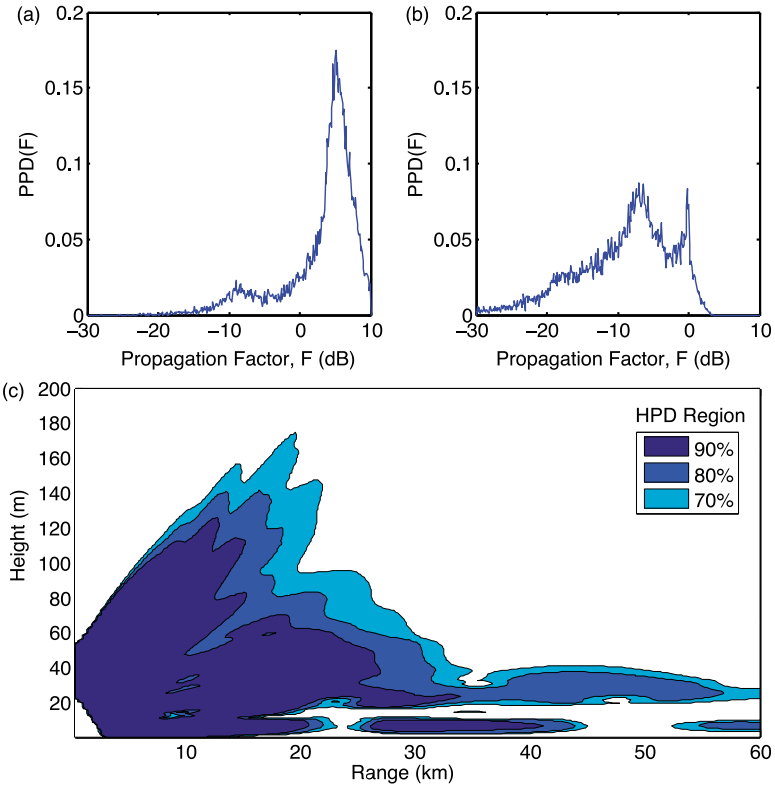

Figure 8. Posterior probability distribution of the propagation loss at range 60 km and altitudes of (a) 28 m, and (b) 180 m above the mean sea level, from the inversion of Figure 6. (c) Detection probability given an isotropic target with an RCS of 1 m^2. © 2006 IEEE. Reprinted, with permission, from *Yardim et al.* [2006].

density (HPD) of the propagation loss obtained from the Metropolis samples of refractivity model parameters from Figure 6. Posterior distributions are shown at a fixed range of 60 km and different altitudes of 28 and 180 m, one inside and one outside the duct. The point inside the duct exhibits a narrow distribution while the variance of the estimated propagation loss outside the duct is much larger. As expected, the detection range increases along the horizon but this increase is not uniform.

[73] Figure 8c shows the effects of uncertainty in the environmental parameters to a simple problem of target detection given that the target is an isotropic antenna with the radar cross section of 1 m^2. The detection threshold in this example is chosen as 35 dB one way loss of the electric field.

[74] A Markov state-space model as discussed by *Vasudevan et al.* [2007] also provides a Bayesian framework by considering the inversion result of the previous states to invert for the current range step.

[75] Continuous temporal and spatial variations in the environment led *Yardim et al.* [2008] to use extended [*Kay*, 1993] and unscented [*Julier et al.*, 2000; *Wan and van der Merve*, 2001] Kalman filters to track RFC results along with Sequential Monte Carlo [*Gordon et al.*, 1993; *Yardim et al.*, 2011] methods such as the particle filters. The paper compared the filter performances in RFC tracking for different types of ducts and computed the Bayesian Cramer-Rao lower bound (CRLB) which presents a lower bound to the RMS error.

[76] *Douvenot et al.* [2010] provided a non-Bayesian approach to inversion but modeled a history of inverted parameters of surface-based ducts to keep the results smooth in azimuthal variations. They considered a library of precomputed propagation losses of candidate profiles to find the one with the minimum distance to the observed clutter. Duct height variations are limited in the latter study and a smoothing procedure on the refractivity profiles is performed after inversions.

4.4. Alternative RFC Formulations

[77] The form of the objective function in (37) suggests that some observations can be weighted more heavily. Usage of different frequencies is discussed in [*Gerstoft et al.*, 2000]. *Gerstoft et al.* [2003a] argued that using a single elevation angle results in inversions with low precision above the duct height. Thus, they used multiple elevation angles of the radar with different weights in the objective function to obtain more robust inversions.

[78] *Rogers et al.* [2005] considered a weighting for the clutter power according to the distance of the range bin from the radar in an evaporation duct. *Zhang et al.* [2011a] suggested using an adaptive weighting algorithm for different range bins in an evaporation duct that depends on the CNR. *Rogers et al.* [2005] have also suggested that RFC should be insensitive to the small variations of peak locations of clutter power with range. Thus, they produced random replica of the predicted field $\mathbf{P}_s$ to make predictions less prone to the measurement errors.

[79] Consideration of an l_2 norm for error of $\Phi(\mathbf{m}) = \|\mathbf{P}_o - \mathbf{P}_s(\mathbf{m})\|^2$ is a consequence of assuming an additive uncorrelated Gaussian noise in (34). The term $\mathbf{n}_r$ in (31) models the noise floor in the receiver which has been modeled by a linear truncation procedure in the logarithmic power domain by *Rogers et al.* [2005] and by a complex Gaussian distribution on the field by *Vasudevan et al.* [2007] and A. Karimian et al. (submitted manuscript, 2011b). A discussion of different random distributions and their effect on RFC is provided by *Yardim et al.* [2009].

[80] Other objective functions have also been suggested in the statistical learning community. l_1 (sum of absolute error terms) and the Huber norm [*Huber*, 1973] are less sensitive to the outliers than the commonly used l_2 norm. The Huber norm is a hybrid of smooth l_2 norm for small errors and robust l_1 treatment of large residuals, which has been used by *Guitton and Symes* [2003] and *Ha et al.* [2009] for the robust inversion of the seismic data.

[81] There have been approaches that do not use the clutter equation as a forward model for inversions. *Barrios* [2004] used a rank correlation approach on the ray tracing results of candidate profiles to invert for the surface-based duct parameters based on the observed clutter power of a 5.6 GHz radar. A tomographic approach using a receiver array at the X-band and correlating the arrival wavefront spectrum to ray traces of candidate profiles has been suggested by *Zhao and Huang* [2011]. In a similar problem, *Park and Fabry* [2011] used radar ground echo at low elevation angles to estimate the vertical gradient of refractivity near the ground. They used ray tracing to model the radar coverage. One shortcoming of the current RFC approaches is evident when surface and weather (volume) clutter are hard to separate such as in precipitation.

5. Conclusion and Future Directions

[82] RFC is an approach to estimate the refractivity structure of a maritime environment based on the observed radar clutter power. Marine ducts and their mathematical models have been discussed, and a framework for casting an inverse problem was presented. An inversion consists of a forward model to map the candidate profiles to the observation domain, and a similarity measure to find the best profile. However, there are several shortcomings in the current approaches to RFC that need to be addressed in future studies:

[83] Bilinear and trilinear approximations to surface-based ducts are not representative of the duct structure in some situations, and their performance worsens as the operational frequency increases. There have been attempts to overcome this problem by suggesting environmental refractivity models that rely on finding basis vectors of the refractivity profile. Models for duct structures are required that are simple (for easy inversion), and at the same time more representative of the true wave propagation, especially if RFC is to be implemented at frequencies higher than 3 GHz.

[84] Sea surface reflectivity models that are currently used in the radar community, e.g. the GIT model, do not represent well the sea reflections at very low grazing angles. Thus, remote sensing problems require more realistic models of the sea surface reflectivity at these angles (<1°).

[85] One of the caveats of RFC algorithms is that detection of elevated ducts is not possible since the trapped electromagnetic waves do not interact with the sea surface. However, these ducts can be predicted based on meteoro-

logical conditions [*Gossard*, 1981]. The 3-D refractivity profiles are intimately linked to the weather. There have been attempts to include climatological statistics of duct heights based on the observation location and time of the year for evaporation ducts [*Yardim et al.*, 2009].

[86] Fusion of weather prediction algorithms with RFC inversions can greatly increase the performance of both. An example is in costal regions when the warm flow of air over the sea forms a rising surface duct for radar propagation. Numerical weather prediction (NWP) systems have undergone substantial development in the last decade. There currently exist capabilities to extract 48 h radar forecast based on output from NWP [*Marshall et al.*, 2008]. These forecasts are used now to predict the radar performance [*LeFurjah et al.*, 2010]. An improvement of RFC then would be using these forecasts [*Haack et al.*, 2010] as prior into the RFC inversion. After the inversion, the RFC posterior refractivity estimates could be used to influence the small-scale data assimilation for NWP. More research is required to fill the gap between weather prediction and RFC.

[87] **Acknowledgments.** This work was supported by SPAWAR under grant N66001-03-2-8938, TDL 0049. The authors would like to thank Dominique Lesselier and Ted Rogers for their constructive comments.

References

Anderson, K. D. (1994), Tropospheric refractivity profiles inferred from low elevation angle measurements of Global Positioning System (GPS) signals, *AGARD Conf. Proc.*, *567*, 2.1–2.7.

Anderson, K. D. (1995), Radar detection of low-altitude targets in a maritime environment, *IEEE Trans. Antennas Propag.*, *43*(6), 609–613, doi:10.1109/8.387177.

Babin, S. M., G. A. Young, and J. A. Carton (1997), A new model of the oceanic evaporation duct, *J. Appl. Meteorol.*, *36*(3), 193–204, doi:10.1175/1520-0450(1997)036<0193:ANMOTO>2.0.CO;2.

Barrios, A. E. (1992), Parabolic equation modeling in horizontally inhomogeneous environments, *IEEE Trans. Antennas Propag.*, *40*(7), 791–797, doi:10.1109/8.155744.

Barrios, A. E. (1994), A terrain parabolic equation model for propagation in the troposphere, *IEEE Trans. Antennas Propag.*, *42*(1), 90–98, doi:10.1109/8.272306.

Barrios, A. E. (2002), Advanced propagation model (APM) computer software configuration item (CSCI), technical document 3145, Space and Nav. Warf. Syst. Cent., San Diego, Calif.

Barrios, A. E. (2003), Considerations in the development of the advanced propagation model (APM) for U.S. Navy applications, in *2003 Proceedings of the International Conference on Radar*, pp. 77–82, IEEE Press, Piscataway, N. J.

Barrios, A. E. (2004), Estimation of surface-based duct parameters from surface clutter using a ray trace approach, *Radio Sci.*, *39*, RS6013, doi:10.1029/2003RS002930.

Barton, D. K. (1988), *Modern Radar System Analysis*, 590 pp., Artech House, Norwood, Mass.

Blake, L. V. (1980), *Radar Range Performance Analysis*, Lexington Books, Lexington, Mass.

Boyer, D., G. Gentry, J. Stapleton, and J. Cook (1996), Using remote refractivity sensing to predict tropospheric refractivity from measurements of microwave propagation, paper presented at Sensor and Propagation Panel Symposium, "Remote Sensing: A Valuable Source of Information," Advis. Group for Aerosp. Res. and Dev., Toulouse, France.

Brooks, I. M., A. K. Goroch, and D. P. Rogers (1999), Observations of strong surface radar ducts over the Persian Gulf, *J. Appl. Meteorol.*, *38*(9), 1293–1310, doi:10.1175/1520-0450(1999)038<1293:OOSSRD>2.0.CO;2.

Budden, K. G. (1961), *The Wave-Guide Mode Theory of Wave Propagation*, Prentice-Hall, Englewood Cliffs, N. J.

Dockery, G. D. (1990), Method for modeling sea surface clutter in complicated propagation environments, *IEE Proc. Part F., Radar Signal Process.*, *137*, 73–79.

Dockery, G. D., and J. R. Kuttler (1996), An improved impedance-boundary algorithm for Fourier split-step solution of the parabolic wave equation, *IEEE Trans. Antennas Propag.*, *44*(12), 1592–1599, doi:10.1109/8.546245.

Dockery, G. D., R. S. Awadallah, D. E. Freund, J. Z. Gehman, and M. H. Newkirk (2007), An overview of recent advances for the TEMPER radar propagation model, in *IEEE Radar Conference*, pp. 896–905, IEEE Press, Boston, doi:10.1109/RADAR.2007.374338.

Dosso, S. E., and J. Dettmer (2011), Bayesian matched-field geoacoustic inversion, *Inverse Probl.*, *27*(5), 055009, doi:10.1088/0266-5611/27/5/055009.

Dougherty, H., and B. A. Hart (1979), Recent progress in duct propagation predictions, *IEEE Trans. Antennas Propag.*, *27*(4), 542–548, doi:10.1109/TAP.1979.1142130.

Douvenot, R., and V. Fabbro (2010), On the knowledge of radar coverage at sea using real time refractivity from clutter, *IET Radar Sonar Navig.*, *4*(2), 293–301, doi:10.1049/iet–rsn.2009.0073.

Douvenot, R., V. Fabbro, P. Gerstoft, C. Bourlier, and J. Saillard (2008), A duct mapping method using least square support vector machines, *Radio Sci.*, *43*, RS6005, doi:10.1029/2008RS003842.

Douvenot, R., V. Fabbro, P. Gerstoft, C. Bourlier, and J. Saillard (2010), Real time refractivity from clutter using a best fit approach improved with physical information, *Radio Sci.*, *45*, RS1007, doi:10.1029/2009RS004137.

Doviak, R. J., and D. S. Zrnić (1993), *Doppler Radar and Weather Observations*, 2nd ed., 562 pp., Academic, San Diego, Calif.

Fabry, F., C. Frush, I. Zawadzki, and A. Kilambi (1997), On the extraction of near-surface index of refraction using radar phase measurements from ground targets, *J. Atmos. Oceanic Technol.*, *14*, 978–987.

Fairall, C. W., E. F. Bradley, D. P. Rogers, J. B. Edson, and G. S. Young (1996), Bulk parametrization of air-sea fluxes for Tropical Ocean-Global Atmosphere Coupled-Ocean Atmosphere Response Experiment, *J. Geophys. Res.*, *101*(C2), 3747–3764, doi:10.1029/95JC03205.

Feit, M. D., and J. A. Fleck (1978), Light propagation in graded-index fibers, *Appl. Opt.*, *17*, 3990–3998, doi:10.1364/AO.17.003990.

Fletcher, C. (1978), Clutter subroutine, *Memo. TSC-W84-01/cad*, Technol. Serv. Corp., Silver Spring, Md.

Frederickson, P. A., K. L. Davidson, and A. K. Goroch (2000a), Operational bulk evaporation duct model for MORIAH, *Tech. Rep. NPS/MR-2000-002*, ver. 1.2, 69 pp., Nav. Postgrad. Sch., Monterey, Calif., 5 May.

Frederickson, P. A., K. L. Davidson, C. R. Zeisse, and C. S. Bendall (2000b), Estimating the refractive index structure parameter (C_n^2) over the ocean using bulk methods, *J. Appl. Meteorol.*, *39*, 1770–1783, doi:10.1175/1520-0450-39.10.1770.

Geman, S., and D. Geman (1984), Stochastic relaxation, Gibbs distributions, and the Bayesian restoration of images, *IEEE Trans. Pattern Anal. Mach. Intell.*, *6*, 721–741, doi:10.1080/02664769300000058.

Gerstoft, P., D. F. Gingras, L. T. Rogers, and W. S. Hodgkiss (2000), Estimation of radio refractivity structure using matched-field array processing, *IEEE Trans. Antennas Propag.*, *48*(3), 345–356, doi:10.1109/8.841895.

Gerstoft, P., L. T. Rogers, W. S. Hodgkiss, and L. J. Wagner (2003a), Refractivity estimation using multiple elevation angles, *IEEE J. Ocean. Eng.*, *28*, 513–525, doi:10.1109/JOE.2003.816680.

Gerstoft, P., L. T. Rogers, J. L. Krolik, and W. S. Hodgkiss (2003b), Inversion for refractivity parameters from radar sea clutter, *Radio Sci.*, *38*(3), 8053, doi:10.1029/2002RS002640.

Gerstoft, P., W. S. Hodgkiss, L. T. Rogers, and M. Jablecki (2004), Probability distribution of low-altitude propagation loss from radar sea clutter data, *Radio Sci.*, *39*, RS6006, doi:10.1029/2004RS003077.

Gingras, D. F., P. Gerstoft, and N. L. Gerr (1997), Electromagnetic matched field processing: Basic concepts and tropospheric simulations, *IEEE Trans. Antennas Propag.*, *42*(10), 1536–1545, doi:10.1109/8.633863.

Gordon, N. J., D. J. Salmond, and A. F. M. Smith (1993), Novel approach to nonlinear/non-Gaussian Bayesian state estimation, *IEE Proc. Part F, Radar Signal Process.*, *140*(2), 107–113, doi:10.1049/ip-f-2.1993.0015.

Gossard, E. E. (1981), Clear weather meteorological effects on propagation at frequencies above 1 GHz, *Radio Sci.*, *16*(5), 589–608, doi:10.1029/RS016i005p00589.

Greenaert, G. L. (2007), Notes and correspondence on the evaporation duct for inhomogeneous conditions in coastal regions, *J. Appl. Meteorol. Climatol.*, *46*(4), 538–543.

Gregers-Hansen, V., and R. Mital (2009), An empirical sea clutter model for low grazing angles, paper presented at Radar Conference, Inst. of Electr. and Electron. Eng., Pasadena, Calif.

Guinard, N., J. Ransone, D. Randall, C. Purves, and P. Watkins (1964), Propagation through an elevated duct: Tradewinds III, *IEEE Trans. Antennas Propag.*, *12*(4), 479–490, doi:10.1109/TAP.1964.1138252.

Guitton, A., and W. W. Symes (2003), Robust inversion of seismic data using the Huber norm, *Geophysics*, *68*(4), 1310–1319, doi:10.1190/1.1598124.

Ha, T., W. Chung, and C. Shin (2009), Waveform inversion using a back propagation algorithm and a Huber function norm, *Geophysics*, *74*(3), R15–R24.

Haack, T., and S. D. Burk (2001), Summertime marine refractivity conditions along coastal California, *J. Appl. Meteorol.*, *40*, 673–687, doi:10.1175/1520-0450(2001)040<0673:SMRCAC>2.0.CO;2.

Haack, T., C. Wang, S. Garrett, A. Glazer, J. Mailhot, and R. Marshall (2010), Mesoscale modeling of boundary layer refractivity and atmospheric ducting, *J. Appl. Meteorol. Climatol.*, *49*, 2437–2457.

Hardin, R. H., and F. D. Tappert (1973), Application of the split-step Fourier method to the numerical solution of nonlinear and variable coefficient wave equations, *SIAM Rev. 15*, 423.

Helvey, R. A. (1983), Radiosonde errors and spurious surface-based ducts, *IEE Proc. Part F, Radar Signal Process.*, *130*(7), 643–648.

Hitney, H. V. (1992), Remote sensing of refractivity structure by direct measurements at UHF, *AGARD Conf. Proc.*, *502*, 1.1–1.5.

Hitney, H. V. (1994), Refractive effects from VHF to EHF. Part A: Propagation mechanisms, in *Propagation Modeling and Decision Aids for Communications Radar and Navigation Systems*, *AGARD Lect. Ser.*, *196*, 4A1–4A13.

Hitney, H. V., and J. H. Richter (1976), Integrated refractive effects prediction system (IREPS), *Nav. Eng. J.*, *88*(2), 257–262.

Horst, M., F. Dyer, and M. Tuley (1978), Radar sea clutter model, in *International IEEE AP/S URSI Symposium*, pp. 6–10, London Inst. of Electr. Eng., London.

Hua, Y., and W. Liu (1998), Generalized Karhunen-Loeve transform, *IEEE Signal Process. Lett.*, *5*(6), 141–142.

Huber, P. J. (1973), Robust regression: Asymptotics, conjectures, and Monte Carlo, *Ann. Stat.*, *1*(5), 799–821.

International Telecommunications Union (1990), Reflection from the surface of the Earth, in *Recommendations and Reports of the CCIR*, vol. 5, *Propagation in Nonionized Media*, *Rep. 1008-1*, Geneva, Switz.

Janaswamy, R. (2001), Radio wave propagation over a nonconstant immittance plane, *Radio Sci.*, *36*, 387–405, doi:10.1029/2000RS002338.

Jensen, F. B., W. A. Kuperman, M. B. Porter, and H. Schmidt (2011), *Computational Ocean Acoustics*, Springer, London.

Jeske, H. (1973), State and limits of prediction methods for radar wave propagation conditions over the sea, in *Modern Topics in Microwave Propagation and Air-Sea Interaction*, edited by A. Zancla, pp. 130–148, D. Reidel, Dordrecht, Netherlands.

Julier, S., J. Uhlmann, and H. F. Durrant-White (2000), A new method for nonlinear transformation of means and covariances in filters and estimators, *IEEE Trans. Autom. Control*, *45*, 477–482, doi:10.1109/9.847726.

Katzin, M., R. W. Bauchman, and W. Binnian (1947), 3- and 9-centimeter propagation in low ocean ducts, *Proc. IRE*, *35*, 891–905.

Kay, S. M. (1993), *Fundamentals of Statistical Signal Processing*, vol. 1, *Estimation Theory*, Prentice Hall, Englewood Cliffs, N. J.

Kerr, D. E. (1951), *Propagation of Short Radio Waves*, McGraw-Hill, New York.

Ko, H. W., J. W. Sari, and J. P. Skura (1983), Anomalous microwave propagation through atmospheric ducts, *Johns Hopkins APL Tech. Dig.*, *4*(2), 12–26.

Konstanzer, G. C., J. Z. Gehman, M. H. Newkirk, and G. D. Dockery (2000), Calculation of the surface incident field using TEMPER for land and sea clutter modeling, in *Low Grazing Angle Clutter: Its Characterization, Measurement and Application*, Rep. RTO-MP-060, pp. 14-1–14-12, NATO Res. and Technol. Org., Laurel, Md.

Kraut, S., R. Anderson, and J. Krolik (2004), A generalized Karhunen-Loeve basis for efficient estimation of tropospheric refractivity using radar clutter, *IEEE Trans. Signal Process.*, *52*(1), 48–59, doi:10.1109/TSP.2003.820297.

Krolik, J. L., and J. Tabrikian (1997), Tropospheric refractivity estimation using radar clutter from the sea surface, paper presented at Battlespace Atmospheric Conference, Space and Nav. Warf. Syst. Cent., San Diego, Calif., 2–4 Dec.

Kukushkin, A. (2004), *Radio Wave Propagation in the Marine Boundary Layer*, Wiley, Weinheim, Germany.

Kuttler, J. R. (1999), Differences between the narrow-angle and wide-angle propagators in the split-step Fourier solution of the parabolic wave equation, *IEEE Trans. Antennas Propag.*, *47*(7), 1131–1140, doi:10.1109/8.785743.

Kuttler, J. R., and R. Janaswamy (2002), Improved Fourier transform methods for solving the parabolic wave equation, *Radio Sci.*, *37*(2), 1021, doi:10.1029/2001RS002488.

LeFurjah, G., R. Marshall, T. Casey, T. Haack, and D. De Forest Boyer (2010), Synthesis of mesoscale numerical weather prediction and empirical site-specific radar clutter models, *IET Radar Sonar Navig.*, *4*(6), 747–754.

Leontovich, M. A., and V. A. Fock (1946), Solution of the problem of electromagnetic wave propagation along the earth's surface by the method of parabolic equation, *Acad. Sci. USSR. J. Phys.*, *10*, 13–23.

Levy, M. (2000), *Parabolic Equation Methods for Electromagnetic Wave Propagation*, Inst. of Electr. Eng., London.

Lin, L., Z. Zhao, Y. Zhang, and Q. Zhu (2011), Tropospheric refractivity profiling based on refractivity profile model using single ground-based global positioning system, *IET Radar Sonar Navig.*, *5*(1), 7–11, doi:10.1049/iet-rsn.2009.0167.

Liu, W. T., K. B. Kataros, and J. A. Businger (1979), Bulk parameterization of air-sea exchanges of heat and water vapor including the molecular constraints at the interface, *J. Atmos. Sci.*, *36*, 1722–1735, doi:10.1175/1520-0469(1979)036<1722:BPOASE>2.0.CO;2.

Lowry, A. R., C. Rocken, S. V. Sokolovsky, and K. D. Anderson (2002), Vertical profiling of atmospheric refractivity from ground-based GPS, *Radio Sci.*, *37*(3), 1041, doi:10.1029/2000RS002565.

MacKay, D. J. C. (2003), *Information Theory, Inference and Learning Algorithms*, Cambridge Univ. Press, Cambridge, U. K.

Marshall, R. E., W. D. Thornton, G. LeFurjah, and S. Casey (2008), Modeling and simulation of notional future radar in non-standard propagation environments facilitated by mesoscale numerical weather prediction modeling, *Nav. Eng. J.*, *120*(4), 55–66, doi:10.1111/j.1559-3584.2008.00165.x.

Mentes, S., and Z. Kaymaz (2007), Investigation of surface duct conditions over Istanbul, Turkey, *J. Appl. Meteorol. Climatol.*, *46*, 318–337, doi:10.1175/JAM2452.1.

Metropolis, N., A. W. Rosenbluth, M. N. Rosenbluth, A. H. Teller, and E. Teller (1953), Equation of state calculations by fast computing machines, *J. Chem. Phys.*, *21*, 1087–1092, doi:10.1063/1.1699114.

Miller, A. R., R. M. Brown, and E. Vegh (1984), New derivation for the rough surface reflection coefficient and for the distribution of the sea-wave elevations, *IEE Proc. Part H, Microwaves Opt. Antennas*, *131*(2), 114–116, doi:10.1049/ip-h-1.1984.0022.

Miller, E. L., and A. S. Willsky (1996a), A multiscale, statistically based inversion scheme for linearized inverse scattering problems, *IEEE Trans. Geosci. Remote Sens.*, *34*(2), 346–357, doi:10.1109/36.485112.

Miller, E. L., and A. S. Willsky (1996b), Wavelet-based methods for the nonlinear inverse scattering problem using the extended Born approximation, *Radio Sci.*, *31*(1), 51–65, doi:10.1029/95RS03130.

Nathanson, F. E., J. P. Reilly, and M. N. Cohen (1991), *Radar Design Principles: Signal Processing and the Environment*, 2nd ed., McGraw-Hill, New York.

Ó Ruanaidh, J. J. K., and W. J. Fitzgerald (1996), *Numerical Bayesian Methods Applied to Signal Processing*, Springer, New York.

Pappert, R. A., R. A. Paulus, and F. D. Tappert (1992), Sea echo in tropospheric ducting environments, *Radio Sci.*, *27*(2), 189–209, doi:10.1029/91RS02962.

Park, S., and F. Fabry (2011), Estimation of near-ground propagation conditions using radar ground echo coverage, *J. Atmos. Oceanic Technol.*, *28*, 165–180, doi:10.1175/2010JTECHA1500.1.

Patterson, W. L. (1987), Historical electromagnetic propagation condition database description, *Tech. Doc. 1149*, Nav. Ocean Syst. Cent., San Diego, Calif.

Paulus, R. A. (1985), Practical application of an evaporation duct model, *Radio Sci.*, *20*, 887–896, doi:10.1029/RS020i004p00887.

Paulus, R. A. (1990), Evaporation duct effects on sea clutter, *IEEE Trans. Antennas Propag.*, *38*(11), 1765–1771, doi:10.1109/8.102737.

Pekeris, C. L. (1946), Accuracy of the Earth flattening approximation in the theory of microwave propagation, *Phys. Rev.*, *70*(7–8), 518–522, doi:10.1103/PhysRev.70.518.

Phillips, O. M. (1985), Spectral and statistical properties of the equilibrium range in wind-generated gravity waves, *J. Fluid Mech.*, *156*, 505–531, doi:10.1017/S0022112085002221.

Rabiner, L. R. (1989), A tutorial on hidden Markov models and selected applications in speech recognition, *Proc. IEEE*, *77*(2), 257–286, doi:10.1109/5.18626.

Reilly, J. P., and G. D. Dockery (1990), Influence of evaporation ducts on radar sea return, *IEE Proc. Part F, Radar Signal Process.*, *137*, 80–88.

Richter, J. H. (1995), Structure, variability, and sensing of the coastal environments, paper presented at Symposium on Propagation Assessment in Coastal Environments, NATO Advis. Group for Aerosp. Res. and Dev., Neuilly-sur-Seine, France.

Roberts, R. D., et al. (2008), REFRACTT 2006: Real time retrieval of high-resolution, low-level moisture fields from operational NEXRAD and research radars, *Bull. Am. Meteorol. Soc.*, *89*(10), 1535–1538.

Rogers, L. T. (1996), Effects of the variability of atmospheric refractivity on propagation estimates, *IEEE Trans. Antennas Propag.*, *44*(4), 460–465, doi:10.1109/8.489297.

Rogers, L. T. (1997), Likelihood estimation of tropospheric duct parameters from horizontal propagation measurements, *Radio Sci.*, *32*, 79–92, doi:10.1029/96RS02904.

Rogers, L. T., and R. A. Paulus (1996), Measured performance of evaporation duct models, *Tech. Rep. 2989*, Nav. Command Control and Ocean Surveill. Cent. Res. and Dev. Test and Eval. Div., San Diego, Calif.

Rogers, L. T., C. P. Hattan, and J. K. Stapleton (2000), Estimating evaporation duct heights from radar sea echo, *Radio Sci.*, *35*(4), 955–966, doi:10.1029/1999RS002275.

Rogers, L. T., M. Jablecki, and P. Gerstoft (2005), Posterior distributions of a statistic propagation loss inferred from radar sea clutter, *Radio Sci.*, *40*, RS6005, doi:10.1029/2004RS003112.

Rowland, J. R., G. C. Konstanzer, M. R. Neves, R. E. Miller, J. H. Meyer, and J. R. Rottier (1996), SEAWASP: Refractivity characterization using shipboard sensors, in *Proceedings of the 1996 Battlespace Atmospherics Conference*, *Tech. doc. 2938*, pp. 155–164, Nav. Command Control and Ocean Surveill. Cent. Res. and Dev. Test and Eval. Div., San Diego, Calif.

Sambridge, M. (1999a), Geophysical inversion with a neighborhood algorithm—I. Searching a parameter space, *Geophys. J. Int.*, *138*, 479–494.

Sambridge, M. (1999b), Geophysical inversion with a neighborhood algorithm—II. Appraising the ensemble, *Geophys. J. Int.*, *138*, 727–746.

Schmidt, R. O. (1986), Multiple emitter location and signal parameter estimation, *IEEE Trans. Antennas Propag.*, *34*(3), 276–280, doi:10.1109/TAP.1986.1143830.

Sittrop, H. (1977), Characteristics of clutter and target at X- and Ku-band, *AGARD Conf. Proc.*, *197*, 28.1–28.27.

Skolnik, M. I. (2008), *Radar Handbook*, 3rd ed., McGraw-Hill, New York.

Skura, J. P., C. E. Schemm, H. W. Ko, and L. P. Manzi (1990), Radar coverage predictions through time- and range-dependent refractive atmosphere with planetary boundary layer and electromagnetic parabolic equation models, in *The Record of the IEEE 1990 International Radar Conference*, pp. 370–378, IEEE Aerosp. and Electron. Syst. Soc., New York.

Tabrikian, J., and J. Krolik (1999), Theoretical performance limits on tropospheric refractivity estimation using point-to-point microwave measurements, *IEEE Trans. Antennas Propag.*, *47*(11), 1727–1734, doi:10.1109/8.814953.

Thomson, D. J., and N. R. Chapman (1983), A wide-angle split-step algorithm for the parabolic equation, *J. Acoust. Soc. Am.*, *74*(6), 1848–1854, doi:10.1121/1.390272.

Vasudevan, S., R. Anderson, S. Kraut, P. Gerstoft, L. T. Rogers, and J. L. Krolik (2007), Recursive Bayesian electromagnetic refractivity estimation from radar sea clutter, *Radio Sci.*, *42*, RS2014, doi:10.1029/2005RS003423.

Von Engeln, A. G., G. Nedoluha, and J. Teixeira (2003), An analysis of the frequency and distribution of ducting events in simulated radio occultation measurements based on ECMWF fields, *J. Geophys. Res.*, *108*(D21), 4669, doi:10.1029/2002JD003170.

Wakimoto, R. M., and M. H. Murphy (2009), Analysis of a dryline during IHOP: Implications for convection initiation, *Mon. Weather Rev.*, *137*(3), 912–936, doi:10.1175/2008MWR2584.1.

Wan, E. A., and R. van der Merve (2001), The unscented Kalman filter, in *Kalman Filtering and Neural Networks*, edited by S. Haykin, John Wiley, New York.

Wandinger, U. (2005), Raman lidar, in *Lidar*, edited by C. Weitkamp, *Springer Ser. Opt. Sci.*, *102*, 241–271.

Wang, B., Z. S. Wu, A. Zhao, and H. G. Wang (2009), Retrieving evaporation duct heights from radar sea clutter using particle swarm optimization, *Prog. Electromagn. Res.*, *9*, 79–91, doi:10.2528/PIERM09090403.

Weckwerth, T. M., C. R. Petter, F. Fabry, S. J. Park, M. A. LeMone, and J. W. Wilson (2005), Radar refractivity retrieval: Validation and application to short-term forcasting, *J. Appl. Meteorol.*, *44*, 285–300, doi:10.1175/JAM-2204.1.

Willitsford, A., and C. R. Philbrick (2005), Lidar description of the evaporation duct in ocean environments, *Proc. SPIE Int. Soc. Opt. Eng.*, *5885*, 140–147.

Wilson, J. W., and R. D. Roberts (2006), Summary of convective storm initiation and evolution during IHOP: Observational and modeling perspective, *Mon. Weather Rev.*, *134*(1), 23–47, doi:10.1175/MWR3069.1.

Yardim, C., P. Gerstoft, and W. S. Hodgkiss (2006), Estimation of radio refractivity from radar clutter using Bayesian Monte Carlo analysis, *IEEE Trans. Antennas Propag.*, *54*(4), 1318–1327, doi:10.1109/TAP.2006.872673.

Yardim, C., P. Gerstoft, and W. S. Hodgkiss (2007), Statistical maritime radar duct estimation using a hybrid genetic algorithm–Markov chain Monte Carlo method, *Radio Sci.*, *42*, RS3014, doi:10.1029/2006RS003561.

Yardim, C., P. Gerstoft, and W. S. Hodgkiss (2008), Tracking refractivity from clutter using Kalman and particle filters, *IEEE Trans. Antennas Propag.*, *56*(4), 1058–1070, doi:10.1109/TAP.2008.919205.

Yardim, C., P. Gerstoft, and W. S. Hodgkiss (2009), Sensitivity analysis and performance estimation of refractivity from clutter techniques, *Radio Sci.*, *44*, RS1008, doi:10.1029/2008RS003897.

Yardim, C., Z. H. Michalopoulou, and P. Gerstoft (2011), An overview of sequential Bayesian filtering in ocean acoustics, *IEEE J. Ocean. Eng.*, *36*(1), 71–89, doi:10.1109/JOE.2010.2098810.

Zhang, J. P., Z. S. Wu, and B. Wang (2011a), An adaptive objective function for evaporation duct estimation from radar sea echo, *Chin. Phys. Lett.*, *28*(3), 034301, doi:10.1088/0256-307X/28/3/034301.

Zhang, J. P., Z. S. Wu, Q. L. Zhu, and B. Wang (2011b), A four-parameter M-profile model for the evaporation duct estimation from radar clutter, *Prog. Electromagn. Res.*, *114*, 353–368.

Zhao, X.-F., and S.-X. Huang (2011), Refractivity estimations from an angle of arrival spectrum, *Chin. Phys. B*, *20*, 029201, doi:10.1088/1674-1056/20/2/029201.

Zhao, X.-F., S.-X. Huang, and H.-D. Du (2011), Theoretical analysis and numerical experiments of variational adjoint approach for refractivity estimation, *Radio Sci.*, *46*, RS1006, doi:10.1029/2010RS004417.

A. E. Barrios, Atmospheric Propagation Branch, Space and Naval Warfare Systems Center, 49170 Propagation Path, San Diego, CA 92152-7385, USA. (amalia.barrios@navy.mil)

P. Gerstoft, W. S. Hodgkiss, A. Karimian, and C. Yardim, Marine Physical Laboratory, Scripps Institute of Oceanography, University of California, San Diego, 9500 Gilman Dr., La Jolla, CA 92037-0238, USA. (gerstoft@ucsd.edu; whodgkiss@ucsd.edu; akarimian@ucsd.edu; cyardim@ucsd.edu)